A Quantum Chemical Study of Comparison of Various Propylene Epoxidation Mechanisms Using H_2O_2 and TS-1 Catalyst

David H. Wells, Jr., Ajay M. Joshi, W. Nicholas Delgass, and Kendall T. Thomson*

School of Chemical Engineering, Purdue University, West Lafayette, Indiana 47907

Received: April 17, 2006; In Final Form: May 31, 2006

We present a comparison of the following prominent propylene epoxidation mechanisms using H_2O_2/TS-1 at a consistent density functional theory (DFT) method: (1) the Sinclair and Catlow mechanism on tripodal site through Ti−OOH species, (2) the Vayssilov and van Santen mechanism on tetrapodal site without Ti−OOH formation, (3) the Munakata et al. mechanism involving peroxy (Ti−O−O−Si) species, (4) the defect site mechanism with a partial silanol nest, and (5) the defect site mechanism with a full silanol nest. We have reproduced the previously published (ethylene epoxidation) pathways (1−3) for propylene epoxidation using larger and SiH_3-terminated cluster models of the T-6 crystallographic site of TS-1. Mechanism 5 is a new mechanism reported here for the first time. The use of a consistent level of theory for all the pathways allows for the first time a meaningful comparison of the energetics representing the aforementioned pathways. We have rigorously identified the important reaction intermediates and transition states and carried out a detailed thermochemical analysis at 298.15 K and 1 atm. On the basis of the Gibbs free energy of activation, the Sinclair and Catlow mechanism ($\Delta G_{act} = 7.9$ kcal/mol) is the energetically most favorable mechanism, which is, however, likely to operate on the *external* surface of TS-1 due to the tripodal nature of the Ti site in their model. The newly reported defect site mechanism (with a full silanol nest) is a competitive propylene epoxidation mechanism. There are two main steps: (1) hydroperoxy formation ($\Delta G_{act} = 8.9$ kcal/mol) and (2) propylene epoxidation ($\Delta G_{act} = 4.6$ kcal/mol). This mechanism is likely to represent the chemistry occurring inside the TS-1 pores in the liquid-phase epoxidation (H_2O_2/TS-1) process and could operate in direct gas-phase epoxidation (H_2/O_2/Au/TS-1) as well. If *only* the propylene epoxidation step is considered, then the Munakata peroxo intermediate (Si−O−O−Ti) is the most reactive intermediate, which can epoxidize propylene with a negligible activation barrier. However, formation of the Munakata intermediate is a very activated step ($\Delta G_{act} = 19.8$ kcal/mol). We also explain the trends in the activation barriers in different mechanisms using geometric and electronic features such as orientation of adsorbed H_2O_2 and propylene, hydrogen bonding, O1−Ti bond distance in the Ti−O1−O2−H intermediate, and O1−O2 stretching in the transition state. Implications of different Ti site models are also discussed in light of the nature of external/internal and nondefect/defect sites of TS-1.

1. Introduction

The Ti-containing MFI-type silicalite (TS-1) was first synthesized at Enichem (Italy).[1] This discovery stimulated the synthesis of several other Ti-containing microporous and mesoporous materials such as TS-1,[1,2] TS-2,[3] Ti-β,[4,5] Ti-MCM-12,[6] Ti-MCM-41,[7,8] and Ti-MCM-48,[9] all of which have been used as catalysts in several reactions of practical interest, e.g., alkane oxidation,[10,11] alkene epoxidation,[12−16] and aromatics hydroxylation.[17] In light of the ongoing efforts for eco-friendly processes, titanosilicates are of interest due to their ability to carry out the aforementioned oxidation reactions using H_2O_2 and/or alkyl hydrogen peroxide under mild conditions, frequently at less than 100 °C.[18,19] These Ti-containing porous catalysts have been characterized in detail using X-ray diffraction, IR, Raman, and UV−vis spectroscopies, and X-ray absorption methods,[20−28] all of which confirm isomorphous substitution of the framework Si by Ti; i.e., Ti ions are tetrahedrally coordinated.

In addition to the eco-friendly nature of H_2O_2/TS-1-catalyzed oxidation reactions, TS-1 is a popular hydrocarbon oxidation catalyst due to its shape selectivity—a result of its small pore size of ∼5.5 Å. Such nanoporous networks inside the TS-1 lattice offer a much higher internal surface area than that available in other titanosilicates with relatively larger pores. Since H_2O_2 can rapidly decompose to water, an efficient use of H_2O_2 toward olefin epoxidation demands very active epoxidation catalysts. TS-1 is a suitable candidate in this respect due to its fast epoxidation kinetics in dilute aqueous H_2O_2 solutions. Clerici et al.[12] have reported initial turn-over frequencies of 1−2 s^{-1} at 40 °C for propylene epoxidation using ∼3.4 wt % H_2O_2. Using dilute solutions of aqueous H_2O_2 in methanol and a TS-1 catalyst, Chen et al.[29] achieved more than 95% selectivity toward propylene oxide (PO) at 40 °C with 92% H_2O_2 selectivity. At 0 °C, both the selectivities were found to be 100%. These studies established the utility of TS-1 in liquid-phase propylene epoxidation.

Due to very high activity and selectivity at mild conditions, liquid-phase epoxidation using H_2O_2/TS-1 is a viable choice for industrial-scale propylene epoxidation.[30] However, this process demands handling large volumes of H_2O_2, and a catalyst with industrially acceptable activity, selectivity, and stability in a direct gas-phase propylene epoxidation process using H_2

* Author to whom correspondance should be addressed. Phone: (765) 496-6706. Fax: (765) 494-0805. E-mail: thomsonk@ecn.purdue.edu.

10.1021/jp062368+ CCC: $33.50
Published on Web 07/07/2006

and O_2 has long been desired. Attempts to use the analogy of ethylene epoxidation in propylene epoxidation with molecular O_2 over Ag/Al_2O_3 catalyst, however, failed due to the presence of allylic H atoms in propylene, which upon facile abstraction result in rapid combustion of propylene to CO_2 and water.[31−33] A breakthrough came from Haruta and co-workers[34] who showed that propylene can be epoxidized with greater than 90% selectivity using gas-phase H_2 and O_2 over a Au/TiO_2 catalyst. Since then, the Haruta lab[35−37] and several other labs[38−47] in the world have made significant contributions in understanding gas-phase propylene epoxidation over Au-based catalysts. Au nanoparticles supported on many Ti-containing supports such as TiO_2,[38,41,48] TS-1,[39,43] Ti-MCM-41,[35] and Ti-MCM-48[36] are active in the gas-phase epoxidation of propylene using H_2 and O_2. However, Au/Ti-based direct gas-phase propylene epoxidation catalysts suffer from activity that is below the commercial standard. Nevertheless, the Au/TS-1 catalyst is an important candidate for a potential commercial gas-phase propylene epoxidation process in the future, not just due to its decent activity and high selectivity, but mainly due to its remarkable stability.[39]

Interestingly, the aforementioned Ti-containing supports (without any supported Au), such as TS-1, are active in liquid-phase propylene epoxidation using H_2O_2. Using electronic density functional theory (DFT) calculations, we found a pathway for H_2O_2 formation from H_2 and O_2 on neutral Au_3[49] and recently extended it further to Au_4^+, Au_5, and Au_5^-.[50] Using inelastic neutron scattering, Goodman and co-workers[51] have provided the first evidence for the formation of OOH and H_2O_2 species on the Au/TiO_2 catalyst using gas-phase H_2 and O_2. The liquid-phase H_2O_2 formation from gaseous H_2 and O_2 has already been reported for Au/Al_2O_3 catalyst suspended in liquid methanol.[52] In light of these studies, it is reasonable to postulate that Au nanoparticles supported on Ti-containing supports (such as TS-1), catalyze the in situ formation of H_2O_2 from H_2 and O_2, which then epoxidizes propylene at the active Ti site(s) of TS-1. It is not unlikely that a similar *propylene epoxidation* mechanism(s) exists for both the gas-phase propylene epoxidation using in situ formed H_2O_2 over Au/TS-1 catalyst and the liquid-phase H_2O_2/TS-1-based propylene epoxidation. Understanding the exact mechanism of propylene epoxidation is, therefore, a key step in the attempts to improve the activity of the TS-1-based catalysts, especially that of the Au/TS-1 catalyst used in the direct gas-phase epoxidation using H_2 and O_2. However, we acknowledge that the mechanism for the direct gas-phase propylene epoxidation using H_2 and O_2 (Au/TS-1 catalyst) may be more complicated and/or quite different than the aforementioned intuitive picture, perhaps due to the presumed proximity and interaction between Au and Ti sites, which is not considered in this study due to absence of Au clusters in our calculations.

Electronic DFT calculations are excellent means of generating hypotheses for reaction mechanism(s) and guiding the subsequent experiments to identify the exact reaction pathway. We[53] and several other researchers[54−63] have employed DFT-based tools to unravel the mechanism of olefin epoxidation using H_2O_2/TS-1. Since it is not feasible to perform the quantum chemical calculations on the whole unit cell of the TS-1 lattice, the calculations are usually performed on a small cluster model of the TS-1 lattice. Typically, such cluster models involve only a few crystallographic T-sites (Ti and Si), and the dangling bonds are frequently terminated with H atoms to satisfy the valencies; i.e., the cluster model is terminated with $-SiH_3$ linkages. To further clarify this issue, we point out that a cluster model with 5 T-sites consists of a central Ti atom, tetrahedrally coordinated to four Si atoms through lattice O atoms, and each of these Si atoms is connected to three H atoms (SiH_3 terminations). To approximate the rigidity of the zeolite framework, the H atoms at the periphery of the cluster models are frequently held fixed in space.

The published olefin epoxidation mechanisms using H_2O_2/TS-1 vary not only in the density functional and the basis set but also in the nature of the cluster model used in the calculation. Generally, the adsorption and activation energies are expected to change when the DFT method and/or the nature of the cluster model is changed; it is not clear whether the differences in the energetics reported are due to inherently different chemistry or due to the DFT methods and cluster models employed. Therefore, a direct comparison of adsorption and activation energies reported in several different olefin epoxidation mechanisms is not as meaningful, and this limitation hampers the computational identification of the most favorable pathway. It is better to compare different hypothesized epoxidation mechanisms at the same level of theory and with a common cluster model that adequately represents the active site. Such an analysis will provide a meaningful comparison of the adsorption energies, activation energies, and hence the rate constants. In addition, many of the previously published studies[56,59,61] involved ethylene instead of propylene, and again a more meaningful comparison can be made by studying all the mechanisms with propylene as a reactant.

In this paper, we report a comparison of several prominent olefin epoxidation mechanisms at the same level of theory; all the pathways were investigated for propylene epoxidation only. More specifically, we used the BPW91/LANL2DZ level of theory in all the calculations and used larger cluster models than that used in the original studies. We note that the usage of better functional (than BPW91) such as B3LYP may change the absolute numbers in the energetics, but the relative trends in a particular mechanism and within a set of mechanisms are not likely to change. We considered full quantum-mechanical (QM) cluster models of T-sites and ignored long-range interactions due to the remainder of the zeolite framework, which could be accounted for by employing a hybrid quantum-mechnical/molecular-mechanical (QM/MM) approach. Again, we postulate that if a sufficiently large full QM cluster model is employed (as done in this study), then due to the relatively small sizes of H_2O_2 and propylene molecules, the relative trends in the energetics are same as those that would be observed in QM/MM calculations. Therefore, we believe that our full QM cluster model approach and the BPW91/LANL2DZ level of theory are good enough to compare the energetics of different olefin epoxidation mechanisms and hence to identify the energetically most favorable mechanism.

Most of the previously published studies reported only the electronic energies evaluated at 0 K in a vacuum. However, more rigorous thermochemical and kinetic data can be extracted by accounting for entropic factors; i.e., the Gibbs free energies of adsorption and activation should be considered for the comparison of different propylene epoxidation mechanisms and hence for selecting the most favorable mechanism. We used Gibbs free energies of activation to identify the most favorable propylene epoxidation mechanism out of five different mechanisms stated in the abstract.

We point out that the geometries reported in the already published papers on mechanisms 1−3 served only as preliminary guides for this study due to the different level of theory employed by us and the need to replace ethylene by propylene;

TABLE 1: Thermochemical Aspects of Various Propylene Epoxidation Mechanisms[e]

mechanism and step	ΔE[a] (kcal/mol)	ΔE_{ZPE}[b] (kcal/mol)	ΔU[c] (kcal/mol)	ΔG[d] (kcal/mol)	pre-exponential factors (s^{-1})
Sinclair and Catlow for External Site					
hydroperoxy formation	7.40	6.37	5.57	7.90	2.69×10^{12}
epoxidation	8.50	7.51	7.15	7.91	1.69×10^{13}
Vayssilov and van Santen					
epoxidation	19.03	17.96	18.37	19.16	4.87×10^{12}
Munakata et al.					
first step in peroxo formation	21.22	20.21	20.44	19.80	6.85×10^{13}
second step in peroxo formation	7.28	6.22	6.90	4.31	9.21×10^{14}
epoxidation	1.20	negligible	1.00	negligible	4.52×10^{14}
Defect (Partial Silanol Nest)					
hydroperoxy formation	15.39	13.71	13.92	14.49	2.89×10^{13}
epoxidation	12.98	12.32	11.89	14.26	7.01×10^{11}
Defect (Full Silanol Nest)					
hydroperoxy formation	10.09	8.83	8.26	8.92	4.45×10^{13}
epoxidation	6.12	5.50	6.53	4.62	7.74×10^{13}
Gas-Phase (Noncatalytic)					
epoxidation	21.09	19.77	18.98	22.40	6.87×10^{11}

[a] The difference in the electronic energies of the transition state and the reactants at 0 K. [b] The difference in the electronic energies of the transition state and the reactants at 0 K with proper accounting of the zero point energy. [c] The difference in the internal energies of the transition state and the reactants at 298 K and 1 atm pressure. [d] The difference in the Gibbs free energies of the transition state and the reactants at 298 K and 1 atm pressure. [e] Note that all the energy differences correspond to the activation energies. Whenever the activation barrier is less than k_BT, it is reported as negligible.

therefore, a rigorous analysis was needed to reproduce mechanisms 1−3. Mechanism 4 is same as that recently published by us, and we simply used the same data with the added Gibbs free energy calculations. However, mechanism 5 is a more complex version of the mechanism 4 and is actually a new mechanism developed by us and reported for the first time. Unless explicitly stated otherwise, all of the energy differences discussed in this paper are from the authors' work. Finally, to the best of our knowledge, ours is the first attempt to compare the kinetic and thermodynamic aspects of several propylene epoxidation mechanisms at a consistent level of theory (and cluster model) and identify the most favorable propylene epoxidation pathway using H_2O_2 as the oxidizing agent and TS-1 as the catalyst.

2. Computational Methods and Cluster Models

All the calculations were conducted using the Gaussian 98 suite of programs.[64] We used electronic DFT with the 1988 exchange functional of Becke[65] and Perdew−Wang's 1991 correlation energy functional (BPW91).[66−68] The Los Alamos LANL2DZ[69,70] effective core pseudopotentials (ECPs) and valence double-ζ basis set for silicon and titanium were utilized as well as the D95[71] full double-ζ basis sets for carbon, hydrogen, and oxygen.

In all the adsorption and reaction steps, we considered several different orientations or starting geometries and carried out full geometry optimization at the aforementioned level of theory; numerous combinations of distances, angles, and solid angles were considered in our search for reaction intermediates and transition states. Thus, we generated an ensemble of different geometries and selected the lowest-energy state, i.e., the ground state, to represent the reaction intermediates in our reaction pathway. In modifying the already published reaction mechanisms to include our choice of propylene as a reactant and a better cluster model, we used the published geometries of reaction intermediates and transition states (for reaction with ethylene) as preliminary guesses in geometry optimizations. We point out that we did not restrict ourselves to only these starting points but also considered many other initial configurations of reaction intermediates and transition states. The changes in the electronic energy at 0 K (ΔE), i.e., the electronic contributions to the activation energies, are reported in Table 1.

The frequency calculations were performed on all the intermediates and transition states. For the case of the stable geometries (energy minima) we verified that all the frequencies are positive, and for the case of the transition states we verified that there is only one imaginary frequency corresponding to the vibration along the reaction pathway. (Corresponding to the constraints on H terminations, there were additional imaginary frequencies for both stable geometries as well as transition states.) These frequency calculations also provided us with the thermochemical analysis at a pressure of 1 atm and a temperature of 298.15 K, which constitute the standard conditions for our analysis. We also report the change in the zero-point-energy (ZPE)-corrected electronic energy, internal energy (ΔU at standard conditions), and Gibbs free energy (ΔG at standard conditions) for the important reaction steps (Table 1). The preexponential factors were calculated using the molecular partition functions as

$$A_{uni} = \frac{k_B T}{h} \frac{Q^{\ddagger}_{TS}}{Q_A}$$

here A_{uni} is the preexponential factor (for the unimolecular reaction), k_B is Boltzmann's constant, h is Planck's constant, T is absolute temperature, Q_A is the partition function per volume of the reactant state A, and $Q^{\ddagger}_{TS}$ is the partition function per volume of the transition state, excluding the vibrational mode corresponding to the reaction coordinate. The details of the calculation of partition functions and other thermodynamic quantities are explained in a book by McQuarrie and Simon.[72] The rate constants at standard conditions can be calculated using the preexponential factors and ZPE-corrected activation energies reported in Table 1.

On the basis of the neutron powder diffraction results,[73] we selected the T-6 crystallographic site for Ti substitution in our calculations. It is interesting to note that the T-6 site is the most favorable candidate for Ti substitution,[73] and due to its location

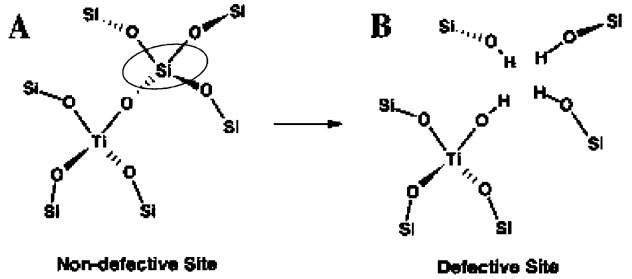

Figure 1. Schematic view of a fully tetrahedrally bonded Ti site substituted for a Si site at one of the lattice positions of TS-1 (A) and the same Ti site located near a silicon vacancy terminated with hydrogen atoms forming a silanol nest (B) (reproduced from ref 53).

at the junction of the straight and sinusoidal channels of the TS-1 lattice, it is also one of the most accessible crystallographic positions. Our T-6 cluster model approximation uses lattice positions from van Koningsveld et al.[74] The selected cluster includes all nearest-neighbor silicon ions and a few selected next-nearest-neighbor silicon ions; depending on the nature of the active Ti site, i.e., external/internal and nondefect/defect, a total of 6−8 T-sites are included in the cluster model. In the entire set of calculations, the cluster model is terminated by substituting H atoms at O atom lattice positions, adjusting their bond lengths to optimized Si−H lengths for our DFT approximation (BPW91/LANL2DZ), and fixing hydrogen positions to crystallographic data during geometry optimization. No oxygen, silicon, or titanium atom locations were fixed during any of these calculations, thus silicon atoms anchored by fixed hydrogen atom positions can be considered "tethered". None of the atoms in propylene was constrained in any way.

Sinclair and Catlow[59] too used H-terminated finite cluster models, however, with only 4 T-sites to model ethylene epoxidation. Noting the size of a propylene molecule, a cluster model with only four sites is inadequate, and a larger model is needed to include all the important interactions in the quantum-mechanical calculations. Both, Vayssilov and van Santen[56] and Munakata et al.[61] used finite cluster models with 5 T-sites and Si−OH terminations to model ethylene epoxidation. However, considering the small size of their cluster model and quite large dipole moments of the O−H bonds, their calculations may include excess contribution due to these O−H bonds over that expected for the actual TS-1 lattice. We employed SiH_3 terminations and avoided the problem of excessive contribution from O−H dipoles. Therefore, we applied our cluster modeling strategy while developing the propylene epoxidation mechanisms based on the previously published results by other researchers.[56,59,61] As stated earlier, we also achieve a consistent comparison of different propylene epoxidation mechanisms.

If all the T-sites of the zeolite are tetrahedrally connected to each other through T−O−T linkages, then the zeolite framework is without any defects. However, even for well-made TS-1, it is possible to find a missing T-atom (defect in the zeolite), which results in the formation of a local silanol nest.[73,75] In Figure 1, we show pictures of nondefect and defect T-sites to clarify the physical situation. We previously reported[53] that it is not unlikely to find approximately one Ti/defect pair (a Ti site with a defect, i.e., missing Si at the neighboring site) per unit cell of TS-1, at 2% Ti substitution level, 8% defect frequency, and random location of Ti substitution and defect occurrences on the Lamberti subset[73] (T-6, T-7, T-11, and T-10). In fact, we also showed that there exists a viable propylene epoxidation mechanism involving a Ti/defect site (with a partial silanol nest) and H_2O_2.[53]

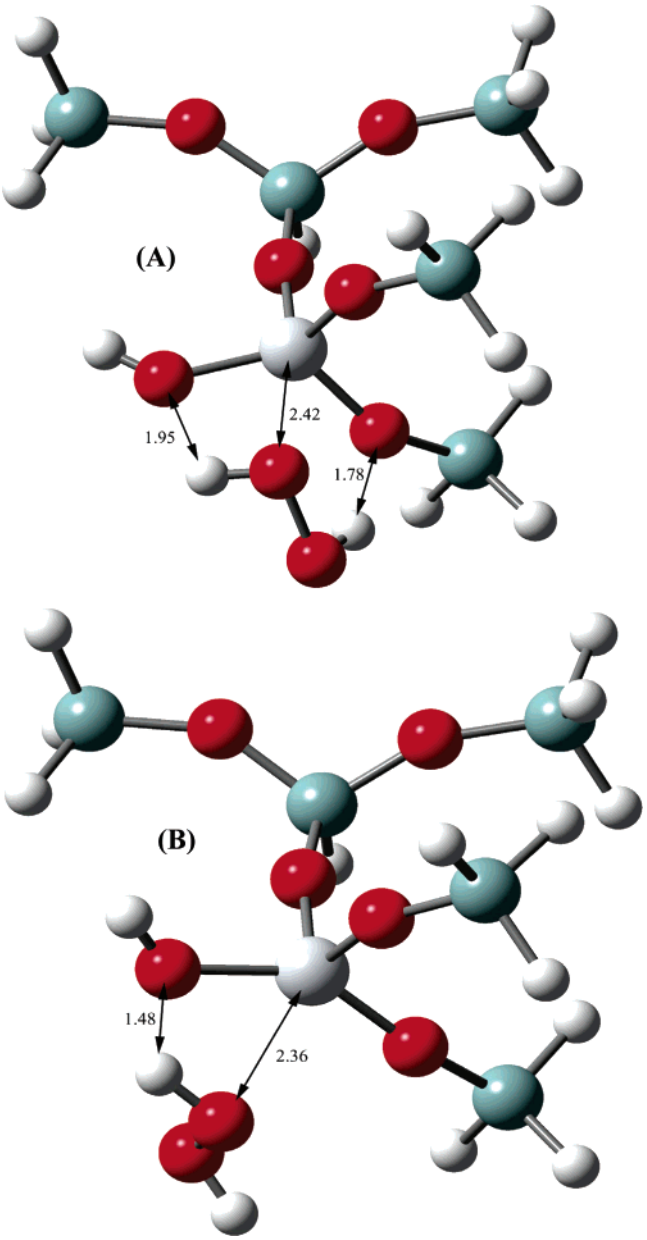

Figure 2. Sinclair and Catlow mechanism on an external surface (partial) site: (A) preadsorbed complex with H_2O_2 and (B) transition-state Complex in formation of the hydroperoxy intermediate. Distances are in angstroms. The color code for all figures is: small white spheres, H atoms; red spheres, O atoms; gray spheres, C atoms; large white spheres, Ti atoms; green spheres, Si atoms.

3. Results

We now discuss our results on different propylene epoxidation mechanisms computed using the BPW91/LANL2DZ level of theory. Rather than analyzing all of the reaction steps involved, only the key transition-state barriers are considered here, since the general picture is already presented in the Introduction and the objective is a consistent comparison of the various competing mechanisms.

3.1. Sinclair and Catlow[59] Mechanism. Sinclair and Catlow performed a computational DFT study of the mechanism first proposed by Bellussi et al.[13] The mechanism for epoxidation of propylene (ethylene in the original work) by H_2O_2 over TS-1 catalysts has two main steps: (1) the formation of the reactive hydroperoxy intermediate from H_2O_2 on the active Ti site in TS-1 and (2) propylene attack on the reactive hydroperoxy

intermediate to form propylene oxide and water. Figure 2A shows the preadsorbed state for H_2O_2 on a Ti site that is only partially connected to the rest of the TS-1 lattice. Such a tripodally anchored Ti site might be found on the exterior termination surface of the TS-1 crystallites. It is also a very crude model of internal sites located adjacent to defect sites. Figure 2A is obviously not even an approximate model for any crystallographically pure tetrahedrally bonded Ti site since the fourth bond to a lattice oxygen has been eliminated.

To form the hydroperoxy (OOH) intermediate on this "partial" site, H_2O_2 first adsorbs via hydrogen bonding to the lattice oxygen of TS-1 and the hydroxyl group on Ti. As shown in Figure 2A, the oxygen atom in H_2O_2, which ultimately bonds to Ti, is also arranged in the coordination sphere of Ti^{4+} at a distance of 2.42 Å. The hydrogen bond distances of 1.78 (to lattice oxygen) and 1.95 (to hydroxyl) Å are typical of this type of bond. The geometry for the transition state in the formation of the hydroperoxy intermediate is shown in Figure 2B. The hydroxyl group that originally completes a tetrahedral coordination sphere on Ti^{4+} receives an H atom from H_2O_2. In the transition state, this bond formation and simultaneous breaking of the H−OOH bond are the main events along the reaction coordinate. The transition-state barrier (change in Gibbs free energy at 298 K) is 7.9 kcal/mol.

The resulting hydroperoxy intermediate of the Sinclair and Catlow mechanism is shown in Figure 3A with propylene adsorbed on the active site. The coordinating water molecule is anchored at 2.16 Å from the Ti center. The water molecule helps to stabilize propylene as the latter adsorbs prior to reaction. The transition state for epoxidation in this mechanism is shown in Figure 3B. To reach to the transition state, propylene has moved toward the front of the complex from the perspective of Figure 3B. Note that Figures 2 and 3 orient the TS-1 cluster model in the same manner allowing for easier comparison of the geometries. The proximal oxygen of the hydroperoxy group is moving toward the carbon−carbon double bond along the reaction coordinate. Like the gas-phase (no catalyst involved) transition state for epoxidation,[53] the transition state for the Sinclair and Catlow mechanism finds the incoming oxygen closer to the terminal carbon of the double bond rather than the central carbon atom in the molecule. The barrier to this transition state is 7.9 kcal/mol (Gibbs free energy difference with respect to the preadsorbed complex).

The two activation barriers (electronic energy difference at 0 K) calculated here for the Sinclair and Catlow mechanism, 7.4 kcal/mol for hydroperoxy formation and 8.5 kcal/mol for epoxidation of propylene, are smaller than those determined by Sinclair and Catlow for the epoxidation of ethylene, respectively, 13.3 and 10.3 kcal/mol. We point out that Sinclair and Catlow did not report Gibbs free energy calculations, and hence we are comparing the activation barriers based on the electronic energy at 0 K. Some of this difference may be accounted for by the difference in the level of DFT theory and the reactant molecule. Sinclair and Catlow used the P86 correlation functional, but PW91[66−68] was used in this research. The same Becke[65] exchange functional was used in both cases. A significant difference in these two studies was the manner in which the rest of the lattice framework was accounted for. In the case of Sinclair and Catlow, the cluster approximation of the Ti site in TS-1 used only 3 or 4 surrounding Si sites. These sites were rigidly fixed in space and terminated with floating H atoms. In the present study, the cluster model is made larger by using the 5 surrounding Si sites, and these sites are free to float in space subject to the constraint of anchoring H atoms,

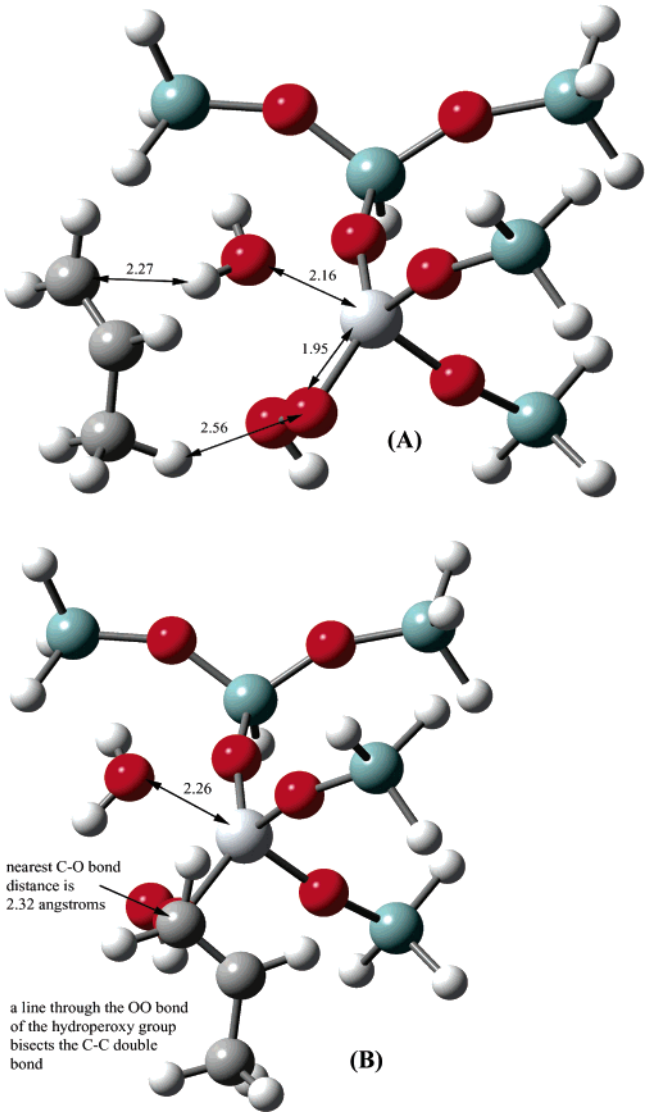

Figure 3. Sinclair and Catlow mechanism on an external surface (partial) site: (A) preadsorbed complex of propylene on the hydroperoxy intermediate and (B) transition-state geometry for epoxidation of propyelene over the hydroperoxy intermediate. Distances are in angstroms.

which were fixed. Sinclair and Catlow constrained the Ti site by fixing 4 Si sites at the next-nearest-neighbor position (two bonds away from Ti), while this study fixed 13 terminal H atoms (effectively 13 Si sites) that were up to five bonds away from Ti. In short, the freedom of the system to respond to changes was greater in the current study, and this together with the other factors accounts for the deviation in calculated energy barriers. The differences in energy barrier height between the Sinclair and Catlow mechanism and the other mechanisms are discussed below.

3.2. Vayssilov and van Santen Mechanism.[56] Another previously studied mechanism of interest is that of Vayssilov and van Santen for ethylene epoxidation. Their proposed mechanism is simpler than that of Sinclair and Catlow since no hydroperoxy intermediate is formed. Instead, they postulated that the preadsorbed complex of H_2O_2 on a Ti active site in TS-1 is sufficiently activated for oxygen to react with an incoming carbon−carbon double bond. The energy barrier in the gas-phase reaction (no catalyst involved) of propylene and H_2O_2 is 22.4 kcal/mol (difference in Gibbs free energy at 298 K).[53] Like the gas-phase reaction, Vayssilov and van Santen's

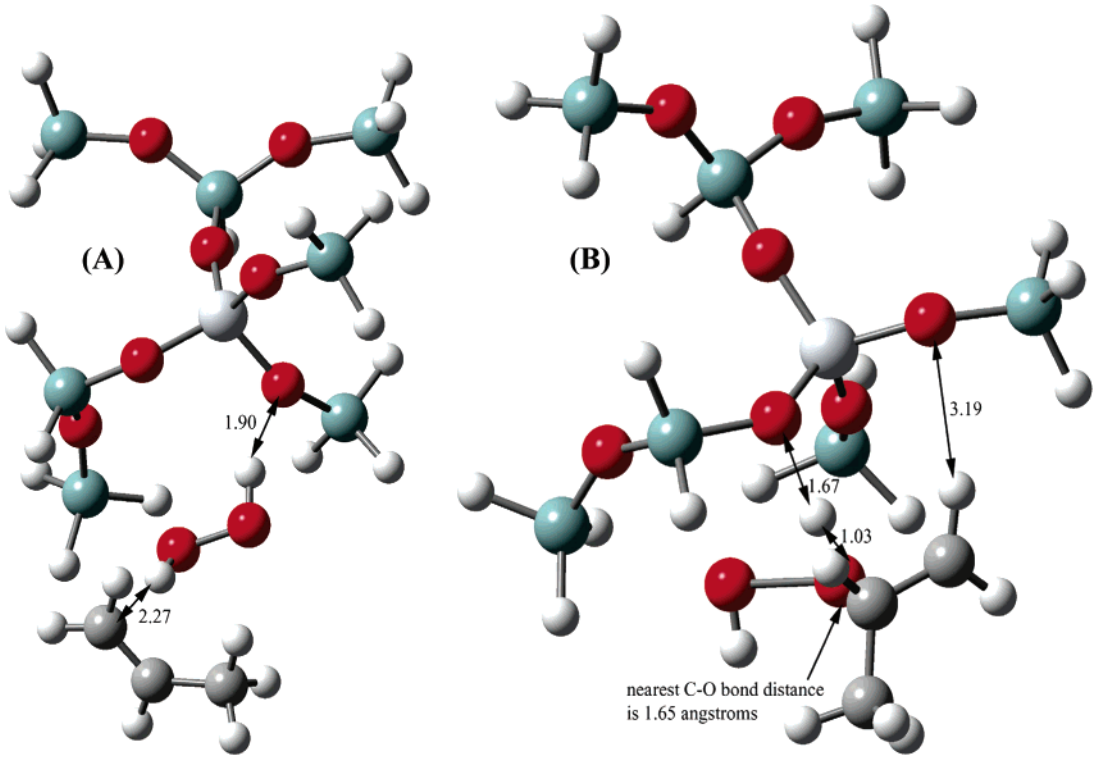

Figure 4. Vayssilov and van Santen mechanism: (A) preadsorbed complex of propylene on adsorbed H_2O_2 and (B) transition-state geometry for epoxidation by adsorbed H_2O_2. Distances are in angstroms.

mechanism yields water and epoxide. One advantage of the Vayssilov and van Santen mechanism is that it is operative over the fully tetrahedral Ti site where all four bonds are to the surrounding lattice oxygen atoms. As shown in Figure 4A, propylene can adsorb on top of the preadsorbed H_2O_2 complex. Figure 4B shows the geometry of the transition-state complex leading to propylene oxide. One of the hydrogens of H_2O_2 is hydrogen-bonding to the lattice oxygen next to the Ti center. This activates the oxygen atom in H_2O_2 such that the transition-state barrier has been lowered from 22.4 to 19.2 kcal/mol (Gibbs free energy difference at 298 K). Again, Vayssilov and van Santen did not report Gibbs free energy calculations. The barrier (19.0 kcal/mol based on electronic energy difference at 0 K) compares well to that reported by Vayssilov and van Santen of 19.8 kcal/mol. The cluster model in this work was larger (total of 8 T-sites) than that employed by Vayssilov and van Santen (total of 5 T-sites), and given the additional flexibility it is not surprising that the energy barrier is slightly reduced. On the basis of our propylene epoxidation calculations using BPW91/LANL2DZ, it is apparent however, that this barrier is well above that for the Sinclair and Catlow mechanism (for external surface sites).

3.3. Munakata et al.[61] Mechanism. Another ethylene epoxidation mechanism was recently proposed by Munakata et al. who postulated a fully tetrahedral Ti site and employed a cluster model with 5 T-sites. In our calculations, we again used a larger cluster model with 8 T-sites and studied propylene epoxidation. Important geometries along this reaction mechanism are illustrated in Figures 5 and 6 and are discussed in turn. For clarity, in Figure 5 we have shown only 5 T-sites with H terminations for all four Si atoms. Actual calculations were performed using a cluster model with 8 T-sites, shown in Figure 6. The energetics of the Munakata et al. mechanism suggest barriers higher than those of the Sinclair and Catlow mechanism. The highest barrier is in the formation of the very reactive Munakata intermediate; once formed however, it reacts with little or no activation barrier.

The Munakata et al. mechanism proceeds through the formation of a reactive Si−O−O−Ti intermediate that can readily epoxidize a carbon−carbon double bond. Formation of the Si−O−O−Ti intermediate requires crossing two energy barriers to accommodate various rearrangements. The starting point geometry with adsorbed hydrogen peroxide is shown in Figure 5A. Hydrogen peroxide is hydrogen-bonded to two of the lattice oxygen atoms surrounding the central Ti center. The Ti coordination sphere is not involved in this initial bonding. At the first transition state shown in Figure 5B, one H atom from H_2O_2 moves to bond with the neighboring lattice oxygen. The resulting stable geometry is illustrated in Figure 5C. An oxygen atom from H_2O_2 is now clearly coordinated in the Ti coordination sphere. The remainder of the H_2O_2 molecule is now essentially in the form of water hydrogen-bonded to the neighboring lattice oxygen. The activation barrier (difference in the Gibbs free energy at 298 K) for this first step is quite high (21.2 kcal/mol). A final minor energy barrier of 4.3 kcal/mol (difference in the Gibbs free energy at 298 K) in the second transition-state geometry (Figure 5D) leads to the unique Si−O−O−Ti peroxy intermediate of Munakata et al. The activated oxygen of the Munakata et al. complex is approximately 1.98 Å from the Ti center. The other oxygen atom in the Si−O−O−Ti bond is approximately 2.00 Å from the Ti center. This complex is remarkably similar to the reactive η-2 hydroperoxy complex first computed by Karlsen and Schöffel.[54] The reactive η-2 hydroperoxy complex in Figure 3A (Sinclair and Catlow mechanism on the defect Ti center) has a Ti−O bond length of 1.95 Å, comparable to the distances in Figure 5D.

Adsorption of propylene on the active Ti site with the peroxo intermediate yields the geometry of Figure 6A. Orientation of the carbon−carbon double bond allows a very easy insertion of oxygen from the high energy Si−O−O−Ti species into the

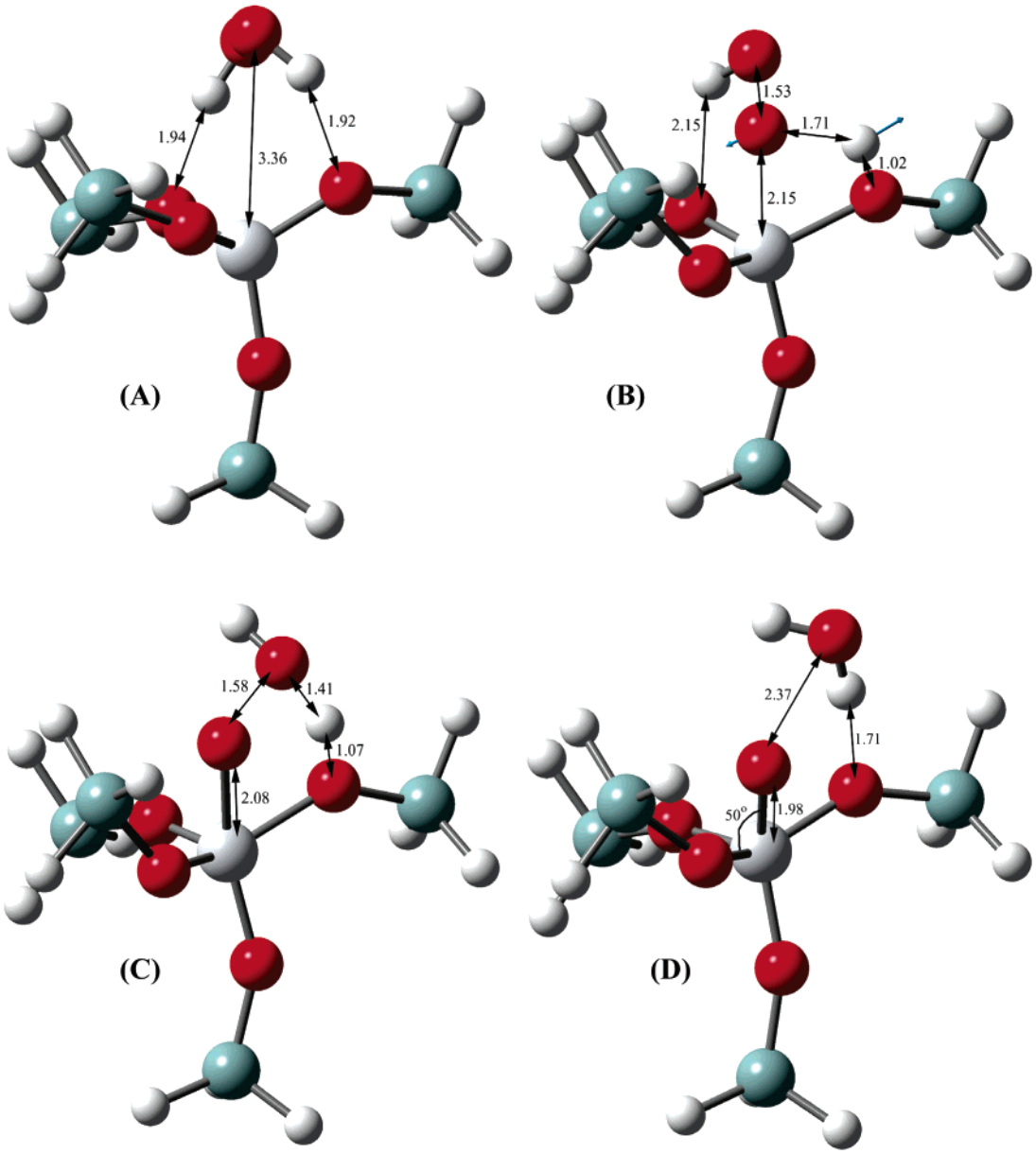

Figure 5. (A) Munakata et al. preadsorbed complex of H_2O_2 on the closed Ti site in TS-1, (B) transition-state geometry for the first step in insertion of oxygen to the peroxo intermediate on the closed Ti site, transition-state motions shown as single-ended arrows without labels, (C) stable intermediate geometry prior to the second step in oxygen insertion to the peroxo intermediate, and (D) transition-state geometry (second step) in oxygen insertion to the peroxo intermediate. Distances are in angstroms.

double bond. Unlike the prior two mechanisms discussed, there is no energy penalty associated with hydroxyl groups stranded by this oxygen insertion; the remaining oxygen of the reactive peroxo complex is close to its equilibrium bond length position, moving only a few tenths of an angstron from transition-state to product geometry. The O−Ti distance changes from 2.00 Å in the transition-state geometry to 1.80 Å in the products (geometries not shown in this paper). This easy accommodation of the end result of epoxidation is the reason that the transition-state energy barrier for this step is so small, 1.2 kcal/mol based on the electronic energy at 0 K and negligibly small based on the Gibbs free energy at 298 K. Formation of this reactive intermediate is energetically demanding, however, compared to alternative mechanisms such as that of Sinclair and Catlow.

3.4. Defect Site Mechanisms. Of the mechanisms discussed so far, Sinclair and Catlow,[59] Vayssilov and van Santen,[56] and Munkata et al.,[61] the energeticly preferred route is that of Sinclair and Catlow. One of the main reasons for this is the fact that the Sinclair and Catlow mechanism assumes that an accessible Ti site is the center of the reaction. In the case of the Vayssilov and van Santen and Munkata et al. mechanisms, the Ti site is fully tetrahedrally bonded to the zeolite lattice framework. The presence of neighboring silicon atoms is a large steric penalty when trying to introduce reactive oxygen species and an olefin around a single Ti center. The Sinclair and Catlow mechanism, however, has not been demonstrated for the closed internal Ti site (tetrahedrally coordinated to four Si sites through lattice oxygens); in fact, we found that this mechanism on such a site does not lead to reactive intermediates.[53] Moreover, Lin and Frei[76] carried out an in situ Fourier transform infrared study of the reaction of gas-phase olefins with TS-1 pretreated with H_2O_2, and their study implies that propylene would react with Ti−OOH formed from H_2O_2/tripodal Ti but would not react with intermediate formed from H_2O_2/tetrapodal Ti.

Is the epoxidation of olefins over TS-1 catalysts confined to external surface reactions at noncrystallographic Ti sites?

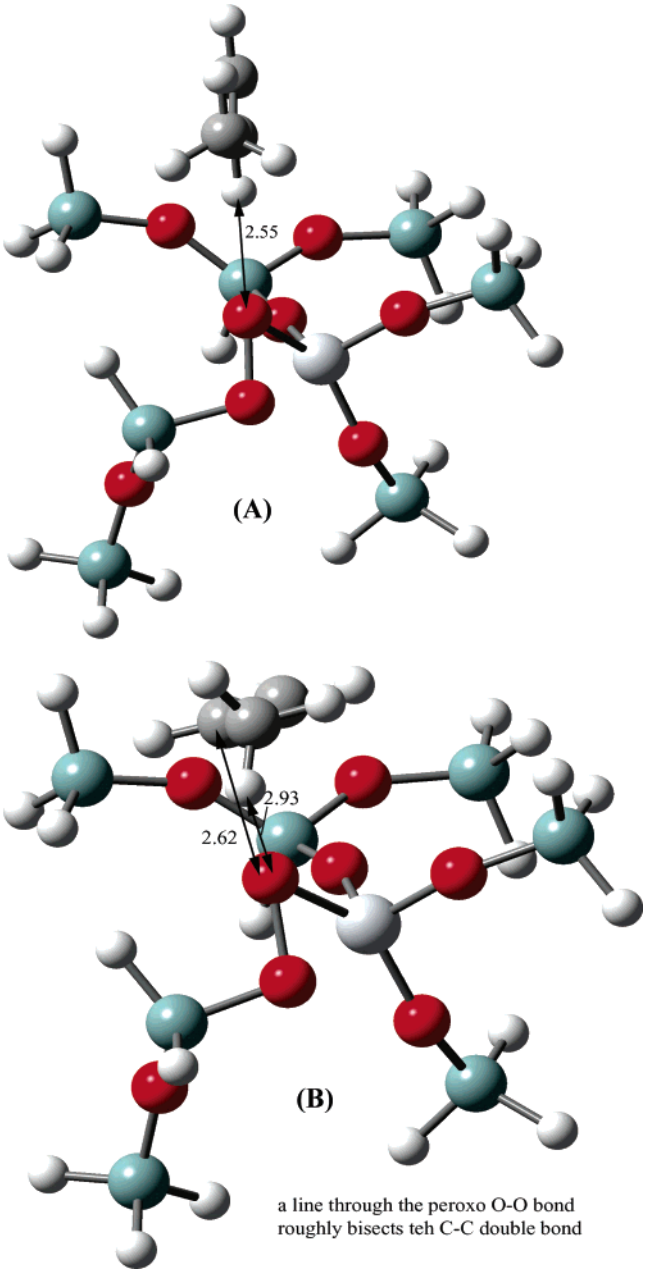

Figure 6. Munakata et al. mechanism: (A) preadsorbed complex of propylene with the peroxo intermediate on the closed Ti site in TS-1 and (B) transition-state geometry during epoxidation of propylene. Distances are in angstroms.

Experimental evidence from the liquid-phase reaction of propylene over TS-1 catalysts suggests that it is not.[14] Recent results from Yap et al.[39] also suggest that both the external surface of Au/TS-1 crystallites as well as their internal (pore) sites are active for epoxidation in the H_2/O_2/propylene system. These considerations prompted the study of Ti/defect sites that might account for reactivity on internal Ti sites. The presence of a defect site in the neighboring position offers some steric freedom for reactions such as the Sinclair and Catlow mechanism to take place. The evidence for this combination of Ti and defect sites was also discussed above (see Lamberti et al.[73]).

3.4.1. Ti/Defect Mechanisms: Partial Silanol Nest Model.[53] The consideration of epoxidation mechanisms with hydroperoxy intermediates located on internal Ti sites leads to a great complication due to the presence of nearby silanol groups. A Ti site with one defect neighbor would mean a total of three neighboring hydroxyl groups within reactive reach of the molecules and groups attached to an active Ti site. The first approximation to this situation was recently reported by us,[53] where only the closest of the neighboring hydroxyls was computed; i.e., only one Si−OH group is modeled instead of three. Although this partial silanol nest is a quite approximate model of the *internal* Ti/defect site, it is actually a reasonable model for the *external* Ti site with a Si−OH neighbor. A good example is seen in Figure 7A, which is the stable adsorbed geometry from H_2O_2 on the Ti/defect site with the defect partially modeled. Hydroxyl groups attached to Ti and Si are well located to allow hydrogen bonding to the H atoms of H_2O_2 on each end of the molecule. Note that the view of the Ti center in Figure 7A is shifted from that in Figures 2−6 to be from the left side of the site as seen in Figures 2−6. The new perspective is maintained in Figures 7 and 8.

The details of the partial nest Ti/defect model are discussed in our recent publication.[53] We only state that the cluster model contains 7 T-sites. The nondefect site model contains 8 T-sites, and due to the loss of one Si site (defect) we have 7 T-sites remaining. We performed additional Gibbs free energy calculations which we discuss here. Of most importance is the size of the energy barriers in each reaction step. Figure 7B shows the transition-state geometry during hydroperoxy intermediate formation (compare this to Figure 2B for the Sinclair and Catlow mechanism on a surface site with no neighboring hindrance). The energy barrier (Gibbs free energy at 298 K) is 14.5 kcal/mol, well above the comparable barrier for Sinclair and Catlow, 7.9 kcal/mol, as computed in this study. A partial explanation of these differences can be seen by noting that the hydroperoxy intermediate formed is an η-1 type rather than the η-2 type seen previously in the Sinclair and Catlow mechanism. The stretched η-1 configuration yields a small energy gain by forming a hydrogen bond between OOH and the adjacent silanol nest.

Adsorption of propylene on the η-1 hydroperoxy intermediate of the Ti/defect (partial) model is shown in Figure 8A. To reach the reaction transition state, the η-1 geometry converts to the more typical η-2 type. This geometry is detailed in Figure 8B. The oxygens in OOH are now 2.11 (reacting) and 2.21 Å from the coordinating Ti site. The motion along the reaction coordinate inserts oxygen into the carbon−carbon double bond. The ensuing sequence of H atom transfers that accommodate the "stranded hydroxyl" group have been discussed in our previous paper.[53] The η-1 to η-2 rearrangement raises the energy barrier in the epoxidation step to 14.3 kcal/mol (Gibbs free energy at 298 K), a level that makes this mechanism unattractive relative to the Sinclair and Catlow mechanism (7.9 kcal/mol for the epoxidation step). However, our partial silanol nest mechanism is energetically more favorable than the Vayssilov and van Santen and Munakata et al. mechanisms.

Until this point, the best mechanism (operating on the external Ti site) is the Sinclair and Catlow mechanism, which has the lowest activation barriers for both the steps. The quest for a reaction mechanism valid on internal Ti sites does not end here; in fact, motivated by the relative success of our partial silanol nest mechanism compared to other "internal" mechanistic explanations such as those of Vayssilov and van Santen and Munakata et al., the partial silanol nest mechanism was next examined with a more complete model of the adjacent silanol nest.

3.4.2. Ti/Defect Mechanisms: Full Silanol Nest Model. Consideration of a more complete silanol nest model yields energy barriers for epoxidation closer to that of Sinclair and Catlow. The silanol nest that heals a Si site defect in a silicalite structure yields three hydroxyl groups, all at a similar distance

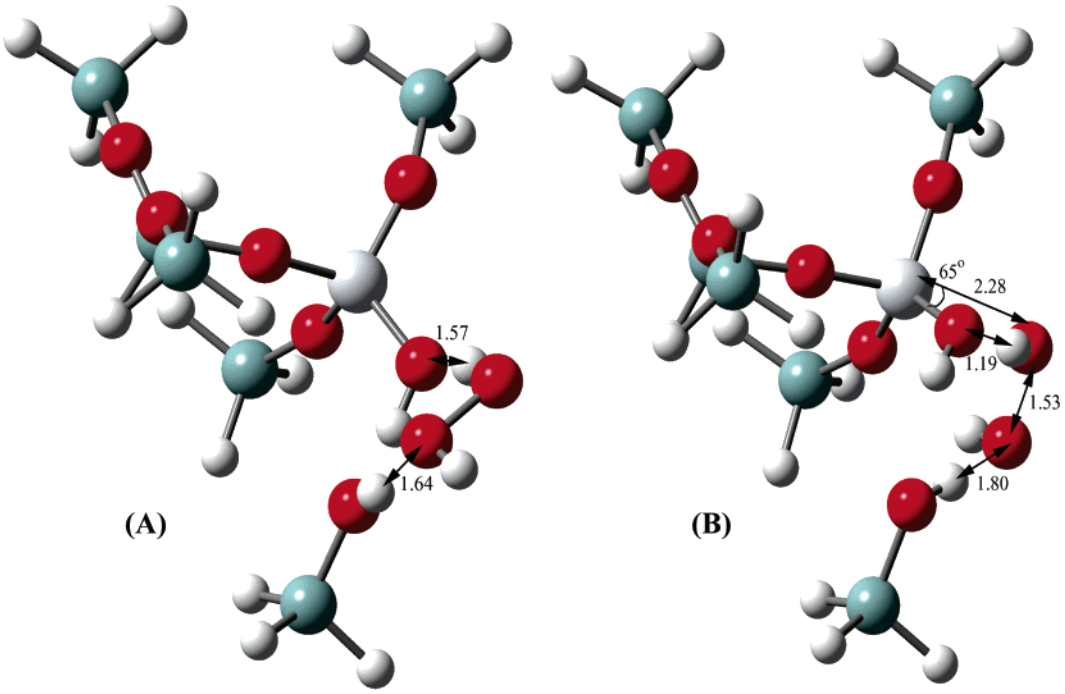

Figure 7. Ti/defect mechanism for the partial silanol nest model: (A) preadsorbed complex of H_2O_2 and (B) transition-state geometry during hydroperoxy intermediate formation. Distances are in angstroms.

to the neighboring Ti center. With a considerable increase in computational requirements, this complication can be treated using the same level of DFT theory previously applied to the mechanisms considered above. Figure 9A gives a good picture of the geometry of this cluster model with three hydroxyl groups of the silanol nest at the left of the figure and the Ti center (labeled) nearby. Again, our cluster model contains six Si sites and one Ti site. As with the partial silanol nest model, H_2O_2 readily bridges the gap between Ti and silanol nest hydroxyls with hydrogen bonds. Formation of the hydroperoxy intermediate goes through the transition-state geometry in Figure 9B, which has an energy barrier of 8.9 kcal/mol (Gibbs free energy at 298 K). This barrier is below that of the partial silanol nest due in part to the ability of the displaced hydroxyl group on the Ti center to find hydrogen bonds in the neighboring silanol nest. The energy barrier of 8.9 kcal/mol is very close to that for the Sinclair and Catlow mechanism (7.9 kcal/mol), and both the pathways represent competitive epoxidation channels. This equivalence is not because the transition state is identical; rather the additional burden of breaking a hydrogen bond between the distal oxygen−hydrogen of H_2O_2 (not needed in the Sinclair and Catlow model) is balanced by the benefit of forming an additional hydrogen bond to the hydroxyl group on Ti (also not present in the simpler Sinclair and Catlow situation).

Water is generated by the formation of the hydroperoxy intermediate. Given the crowded chemical neighborhood of the hydroperoxy intermediate it was found that unless this water molecule was removed the approach of propylene to the reactive oxygen was not possible. It is tempting to now mention the important role that appears to be played by hydrophobicity[77] in the experimental observations of epoxidation in these systems. The relatively weak interaction of water in these systems means that it will be expelled from the zeolite in favor of joining the bulk solvent.

Once water is removed from the active site, propylene can adsorb in the geometry of Figure 10A prior to reaction. The hydroperoxy intermediate is in an η-2 configuration, and the neighboring hydroxyls of the silanol nest are positioned to accommodate the resulting fragment from OOH (i.e., the OH group) after insertion of oxygen to the carbon−carbon double bond. This accommodation is clearly seen in the transition-state geometry of Figure 10B. The energy barrier at the transition state is only 4.6 kcal/mol (Gibbs free energy at 298 K). This is a much smaller barrier than that for the Sinclair and Catlow mechanism (7.9 kcal/mol). Comparison of this transition state to that in the partial nest model indicates that the octahedrally coordinated complex of oxygen atoms around the Ti center is not observed. Rather, the typical η-2 configuration of oxygen atoms forms, which is best described as a tetrahedral complex with an additional oxygen atom on one of the tetrahedral faces.

4. Discussion

A summary of our findings is shown in Table 1 where the energy barriers for all potential rate-limiting steps are shown for all of the mechanisms considered above. It is a compilation of critical information developed for propylene epoxidation by H_2O_2 over TS-1. Trends in the height of the transition-state energy barrier (and hence a main factor in determining reaction rates) can be understood by comparing features of these chemical environments.

The Munakata et al. intermediate, Si−O−O−Ti, is by far the most reactive epoxidizing agent considered in this work. Once formed, its reaction with propylene, assuming the olefin is properly positioned, proceeds with almost no energy barrier. This is in sharp contrast to the gas-phase (noncatalytic) reaction barrier between H_2O_2 and propylene.[53] There are many differences between these two transition states. First, the O−O bond distance at the epoxidation transition state for the Munakata et al. intermediate, 1.65 Å (Table 2), is shorter than that for any other computed intermediate and well below the gas-phase bond distance at the transition state, 2.00 Å. The degree of O−O bond breakage can be seen by comparison with the O−O bond distance computed for the gas-phase molecule of 1.54 Å. Significantly less energy is employed to stretch the O−O bond to reach the Munakata et al. transition state. The Munakata et

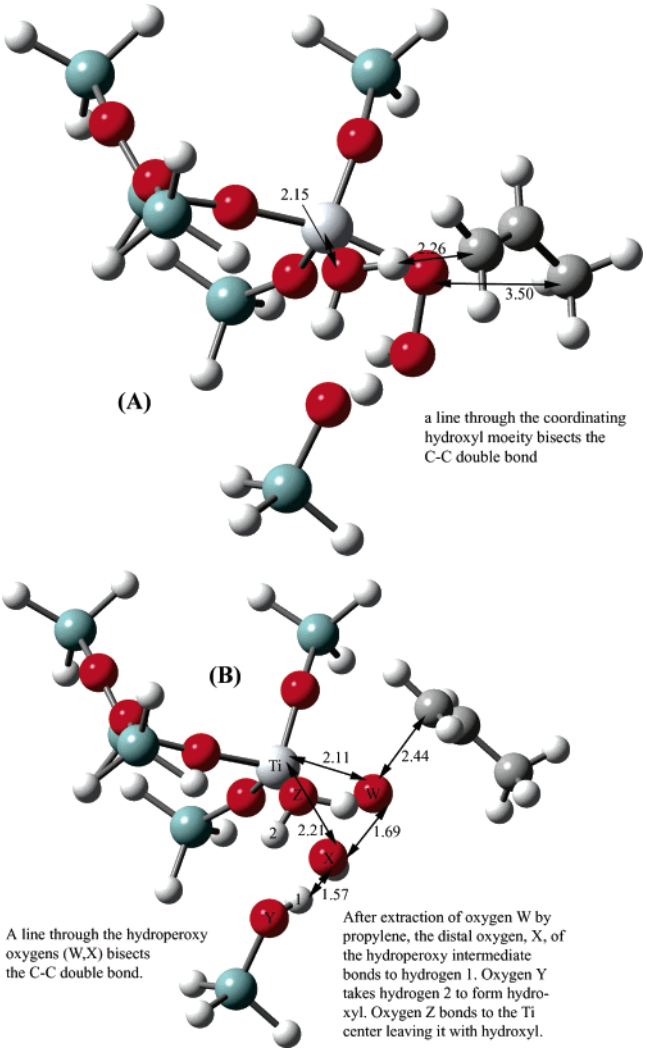

Figure 8. Ti/defect mechanism for the partial silanol nest model: (A) preadsorbed complex of propylene on the hydroperoxy intermediate and (B) transition-state geometry during epoxidation of propylene on the Ti/defect site in TS-1. Distances are in angstroms.

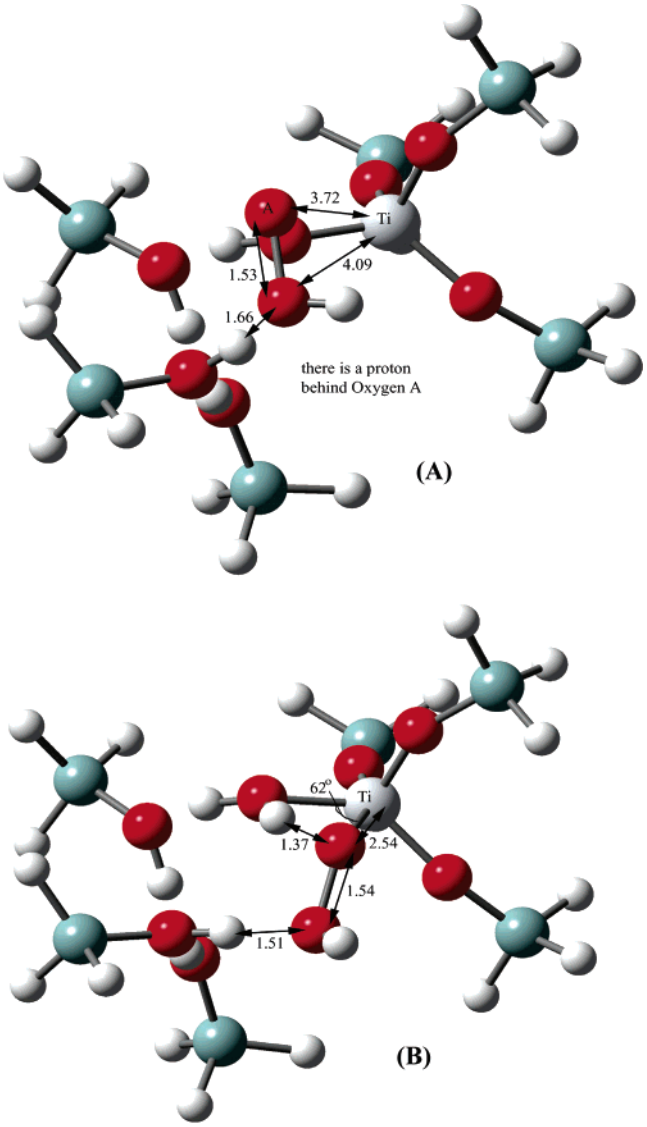

Figure 9. Ti/defect mechanism for the full silanol nest model: (A) preadsorbed complex of H_2O_2 on the Ti site of TS-1 and (B) transition-state geometry during formation of the hydroperoxy intermediate on the Ti site of TS-1. All distances are in angstroms.

al. transition state has another great advantage over all the other mechanisms considered; it essentially leaves no stranded chemical groups, such as hydroxyl groups, far from their ultimate positions. Thus not only is the bond breakage requirement for the Munakata et al. intermediate low, the energetic benefits of bond formation are relatively high for this intermediate. The oxygen atom left after oxygen insertion to the carbon−carbon double bond is only 0.2 Å away from its ultimate O−Ti bond length. In short, the high reactivity predicted for the Munakata intermediate compared to the gas-phase H_2O_2 oxidant is quite understandable.

The next most reactive intermediate is the hydroperoxy intermediate, here considered in three flavors: Sinclair and Catlow (external surface Ti site),[59] Ti/defect (partial nest, simplified model),[53] and Ti/defect (full nest model). The energy barrier (difference in the Gibbs free energy at 298 K) for the reaction of propylene with the hydroperoxy intermediate ranges from 4.6 to 14.3 kcal/mol. Like the Munakata intermediate, the O−O bond stretch at the transition state is a key determinant of the height of the reaction barrier. For all the hydroperoxy intermediates the O−O bond stretch is less than that required for the gas-phase (noncatalytic) reaction of propylene and H_2O_2.[53] Consequently, all the energy barriers are lower than that for the noncatalytic gas-phase reaction. (These are all catalytic reactions.) The significant variations within this group can be explained by closer comparison of the individual chemical environments in each transition state. A secondary driver for the height of the barrier is proximity of the oxygen atoms in OOH to the coordination sphere of Ti^{4+}. The coordination sphere effect is stronger (shorter bond lengths) for the Ti/defect (full silanol nest) intermediate that has the lowest barrier height. The O1−Ti distance (Ti−O1−O2−H) is 1.88 versus 1.99 Å for the Sinclair and Catlow intermediate (next highest barrier height) and 2.11 Å for the Ti/defect (partial silanol nest) model. The Ti^{4+} coordination sphere accommodates electron density from HO−O and reduces the energy required to stretch the O−O bond at the transition-state geometry. A secondary factor that can either help or hinder the reaction is the influence of hydrogen bonding of the hydroperoxy intermediate. When hydrogen bonding is positioned to accommodate the reaction by stabilizing the reactive intermediate it can lower the energy barrier that the "stranded" hydroxyl group must cross to establish a new HO−Ti bond. Perhaps because of the environmental stabilization of the OOH moiety, the O−O bond stretch needed to reach the reactive point of the transition state

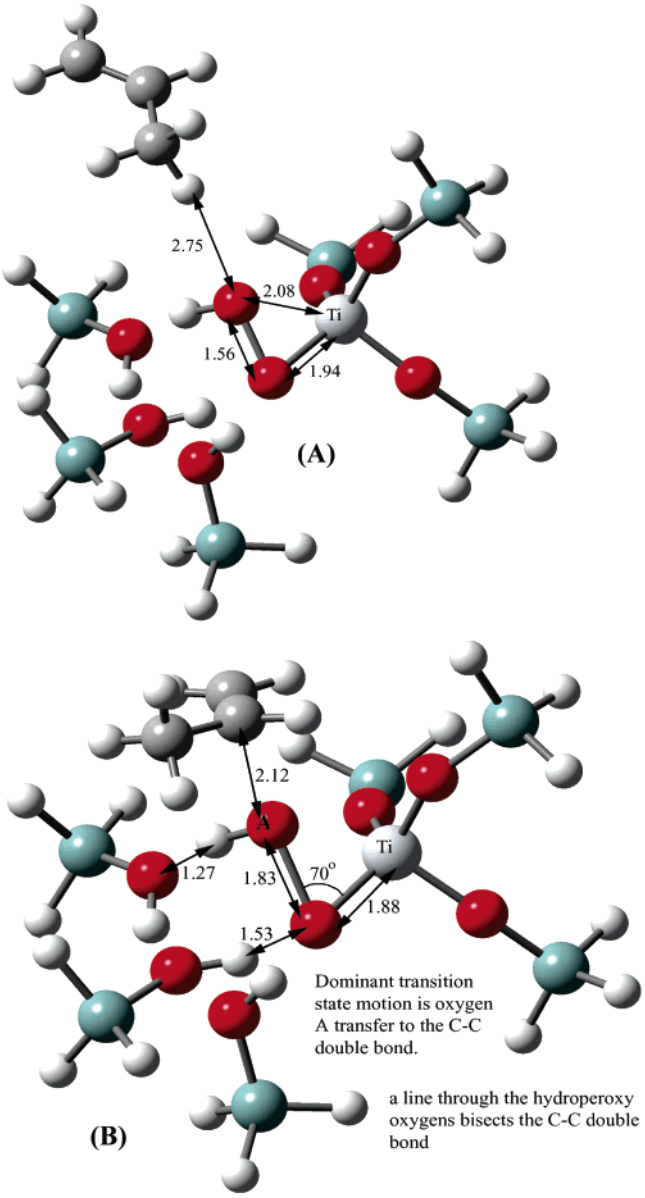

Figure 10. Ti/defect mechanism for the full silanol nest model: (A) preadsorbed complex of propylene on the hydroperoxy intermediate and (B) transition-state geometry during epoxidation of propylene. All distances are in angstroms. The coordinating water molecule has been removed (Figure 9).

is more severe in the Ti/defect (full silanol nest) system. Directionally, the hydrogen bonding stabilization of the hydroperoxy intermediate acts much like the H atoms attached to H_2O_2. The case where hydrogen bonding is detrimental to the overall barrier height is seen in the case for Ti/defect (partial silanol nest). The partial nest model, which is admittedly approximate, stretches the hydroperoxy intermediate into the η-1 configuration. Removal of the oxygen atoms from the helpful influence of the Ti^{4+} coordination sphere raises the barrier height for epoxidation. This effect makes the Ti/defect (partial silanol nest) even less reactive than the Sinclair and Catlow intermediate, which avoids the hydrogen bonding issue altogether due to the empty local environment.

The transition state that most closely resembles the transition state of the gas-phase[53] (noncatalytic) reaction is the Vayssilov and van Santen[56] intermediate, which is H_2O_2 chemisorbed on the Ti center of TS-1. The minor perturbation of the electronic structure of H_2O_2 by the Ti center gives only a slight reduction

TABLE 2: Summary of Transition-State Parameters for All Mechanisms in the Epoxidation Step (Formation of Propylene Oxide)[a]

		bond distances (Å)					
		octahedral complex			nearest H-bond		
mechanism	TS energy barrier (kcal/mol)	O1−Ti	O2−Ti	O−O	O	H	nearest O−C
Munakata	negligible	1.97	1.99	1.65	NA	NA	2.62
defect (full nest)	4.62	1.88	2.12	1.83	1.53	1.27	2.12
Sinclair and Catlow	7.91	1.99	2.17	1.72	2.45	2.83	2.32
defect (partial nest)	14.26	2.11	2.21	1.69	1.57	2.45	2.37
Vayssilov and van Santen	19.16	3.71	3.95	2.04	2.03	1.67	1.65
gas-phase (noncatalytic)	22.40	NA	NA	2.00	NA	1.75	1.75

[a] Note that the hydroperoxy intermediate is represented as Ti−O1−O2−H. Therefore, O1 is the proximal (to the Ti atom) oxygen atom and O2 is the distal oxygen atom.

in the height of the energy barrier for this mechanism versus the gas phase, 19.2 versus 22.4 kcal/mol. The O−O bond stretch required for the chemisorbed H_2O_2 is approximately the same as that for the gas-phase reaction, 2.04 versus 2.00 Å for the gas-phase. Apparently the coordination sphere of Ti^{4+} is able to reduce electron density on the peroxidic oxygens enough to slightly reduce the energy required for the large degree of O−O stretch. Hydrogen bonding of the H_2O_2 hydrogen atoms to the lattice oxygen also reduces the bonding electron density on the reaction center.

5. Conclusions

We compared five different propylene epoxidation mechanisms at the same level of theory. It turns out that all the mechanisms are indeed catalytic; i.e., the activation barriers are lower than that in the gas-phase reaction of propylene and H_2O_2. For *internal* Ti sites, on the basis of the Gibbs free energy analysis at 298 K, we conclude that the newly presented Ti/defect site (with a full silanol nest) pathway is energetically the most favorable candidate to represent the propylene epoxidation chemistry in H_2O_2/TS-1 and perhaps in H_2/O_2/Au/TS-1 catalytic systems. The activation barrier ($\Delta G_{act} = 8.9$ kcal/mol) for the formation of the hydroperoxy intermediate is the rate determining step (RDS) of this pathway. Interestingly, this barrier is quite close to that for the RDS (hydroperoxy formation) of the Sinclair and Catlow mechanism ($\Delta G_{act} = 7.9$ kcal/mol). We point out that the nature of the active Ti site in the cluster models is such that the Sinclair and Catlow mechanism better represents the chemistry occurring on *external* Ti sites. Therefore, Sinclair and Catlow and Ti/defect (with full silanol nest) mechanisms are two competitive propylene epoxidation channels and are significantly more favorable than the other three pathways discussed earlier.

By comparison of the various features of different chemical environments in different mechanisms, it is possible to rationalize the trends in the height of the transition-state energy barrier. We noticed that the stretching of the O−O bond of the Ti−OOH in the transition state for epoxidation is significantly different in different mechanisms. In fact, an η-2 kind of arrangement is favorable for the propylene epoxidation step. Approach of the proximal (to Ti) O atom of H_2O_2 in the coordination sphere of Ti^{4+} is an important feature affecting the activation barriers. We also identified the effect of hydrogen bonding with the lattice oxygen atoms and/or silanol groups as a secondary factor affecting the barrier to the formation of hydroperoxy intermediates.

In light of the activity in the actual epoxidation step, the Munakata et al. intermediate (Ti−O−O−Si) is much better than the hydroperoxy intermediates formed in other mechanisms. However, formation of the Munakata et al. intermediate requires a highly activated step as found in this study. The exciting implication is that propylene epoxidation might be carried out with an almost negligible barrier if we can design/modify a TS-1 catalyst to generate a nontrivial concentration of the Ti−O−O−Si sites. It will be interesting to carry out experiments that involve either a pretreatment or an in situ treatment of the TS-1 catalyst that may aid formation of the Munakata et al. peroxo intermediate.

Acknowledgment. D.H.W. thanks the Shell Oil Company for fellowship funding. This work was also funded through the National Science Foundation Grant No. CTS-0238989-CAREER (K.T.T.). Computational resources were obtained through a grant from the National Computational Science Alliance (AAB Proposal No. ESC030001) and through supercomputing resources at Purdue University. We also acknowledge support by the United States Department of Energy, Office of Basic Energy Sciences through Grant No. DE-FG02-01ER-15107 (W.N.D.). A.M.J. thanks Yogesh Joshi and Thomas Manz for helpful discussions on thermochemistry.

References and Notes

(1) Taramasso, T.; Perego, G.; Notari, B. U. S. Patent 4,410,501, 1983.
(2) van der Pol, A. J. H. P.; van Hooff, J. H. C. *Appl. Catal., A* **1992**, *92*, 93.
(3) Reddy, J. S.; Kumar, R.; Ratnasamy, P. *Appl. Catal.* **1990**, *58*, L1.
(4) Corma, A.; Camblor, M. A.; Esteve, P.; Martinez, A.; Pérez Pariente, J. *J. Catal.* **1994**, *145*, 151.
(5) Camblor, M. A.; Corma, A.; Martínez, A.; Pérez Pariente, J. *J. Chem. Soc., Chem. Commun.* **1992**, 589.
(6) Tuel, A. *Zeolites* **1995**, *15*, 236.
(7) Corma, A.; Navarro, M. T.; Pérez Pariente, J. *J. Chem. Soc., Chem. Commun.* **1994**, 147.
(8) Blasco, T.; Corma, A.; Navarro, M. T.; Pérez Pariente, J. *J. Catal.* **1995**, *156*, 65.
(9) Serrano, D. P.; Li, H.-X.; Davis, M. E. *J. Chem. Soc., Chem. Commun.* **1992**, 745.
(10) Huybrechts, D. R. C.; De Bruycker, L.; Jacobs, P. A. *Nature* **1990**, *345*, 240.
(11) Tatsumi, T.; Nakamura., M.; Negishi, S.; Tominaga, H. *J. Chem. Soc., Chem. Commun.* **1990**, 476.
(12) Clerici, M. G.; Bellussi, G.; Romano, U. *J. Catal.* **1991**, *129*, 159.
(13) Bellussi, G.; Carati, A.; Clerici, M. G.; Maddinelli, G.; Millini, R. *J. Catal.* **1992**, *133*, 220.
(14) Clerici, M. G.; Ingallina, P. *J. Catal.* **1993**, *140*, 71.
(15) Khouw, C. B.; Dartt, C. B.; Labinger, J. A.; Davis, M. E. *J. Catal.* **1994**, *149*, 195.
(16) Langhendries, G.; De Vos, D. E.; Baron, G. V.; Jacobs, P. A. *J. Catal.* **1999**, *187*, 453.
(17) Tuel, A.; Moussa-Khouzami, S.; Taarit, Y. B.; Naccache, C. *J. Mol. Catal.* **1991**, *68*, 45.
(18) Notari, B. *Adv. Catal.* **1996**, *41*, 253.
(19) Arends, I. W. C. E.; Sheldon, R. A.; Wallau, M.; Schuchardt, U. *Angew. Chem.* **1997**, *36*, 1144.
(20) Reddy, J. S.; Sivasanker, S.; Ratnasamy, P. *J. Mol. Catal.* **1991**, *69*, 383.
(21) Blasco, T.; Camblor, M. A.; Corma, A.; Perez Pariente, J. *J. Am. Chem. Soc.* **1993**, *115*, 11806.
(22) Bellussi, G.; Fatore, V. *Stud. Surf. Sci. Catal.* **1991**, *69*, 79.
(23) Pei, S.; Zajak, G. W.; Kaduck, J. A.; Faber, J.; Boyanov, B. I.; Duck, D.; Fazzini, D.; Morrison, T. I.; Yang, D. S. *Catal. Lett.* **1993**, *21*, 333.
(24) Bordiga, S.; Coluccia, S.; Lamberti, C.; Marchese, L.; Zecchina, A.; Boscherini, F.; Buffa, F.; Genoni, F.; Leofanti, G.; Petrini, G.; Vlaic, G. *J. Phys. Chem.* **1994**, *98*, 4125.
(25) Davis, R. J.; Liu, Z.; Tabora, J. E.; Wielband, W. S. *Catal. Lett.* **1995**, *34*, 101.
(26) Feher, F. J.; Newman, D. A.; Walzner, J. F. *J. Am. Chem. Soc.* **1989**, *111*, 1741.
(27) Zecchina, A.; Bordiga, S.; Lamberti, C.; Ricchiardi, G.; Scaranto, D.; Petrini, G.; Leofanti, G.; Mantegazza, M. *Catal. Today* **1996**, *32*, 97.
(28) Duprey, E.; Beaunier, P.; Springuel-Huet, M.-A.; Bozon-Verduraz, F.; Fraissard, J.; Manoli, J.-M.; Brégeault, J.-M. *J. Catal.* **1997**, *165*, 22.
(29) Chen, L. Y.; Chuah, G. K.; Jaenicke, S. *J. Mol. Catal. A* **1998**, *132*, 281.
(30) *Chem. Eng. Prog.* **2003**, (October), 14.
(31) Cant, N. W.; Hall, W. K. *J. Catal.* **1978**, *52*, 81.
(32) Imachi, M.; Egashira, M.; Kuczkowski, R. L.; Cant, N. W. *J. Catal.* **1981**, *70*, 177.
(33) Akimoto, M.; Ichikawa, K.; Echigoya, E. *J. Catal.* **1982**, *76*, 333.
(34) Hayashi, T.; Tanaka, K.; Haruta, M. *J. Catal.* **1998**, *178*, 566.
(35) Uphade, B. S.; Yamada, Y.; Akita, T.; Nakamura, T.; Haruta, M. *Appl. Catal., A* **2001**, *215*, 137.
(36) Uphade, B. S.; Akita, T.; Nakamura, T.; Haruta, M. *J. Catal.* **2002**, *209*, 331.
(37) Qi, C.; Okumura, M.; Akita, T.; Haruta, M. *Appl. Catal., A* **2004**, *263*, 19.
(38) Stangland, E. E.; Stavens, K. B.; Andres, R. P.; Delgass, W. N. *J. Catal.* **2000**, *191*, 332.
(39) Yap, N.; Andres, R. P.; Delgass, W. N. *J. Catal.* **2004**, *226*, 156.
(40) Taylor, B.; Lauterbach, J.; Delgass, W. N. *Appl. Catal., A* **2005**, *291*, 188.
(41) Stangland, E. E.; Taylor, B.; Andres, R. P.; Delgass, W. N. *J. Phys. Chem. B* **2005**, *109*, 2321.
(42) Cumaranatunge, L.; Delgass, W. N. *J. Catal.* **2005**, *232*, 38.
(43) Nijhuis, T. A.; Huizinga, B. J.; Makkee, M.; Moulijn, J. A. *Ind. Eng. Chem. Res.* **1999**, *38*, 884.
(44) Mul, G.; Zwijnenburg, A.; van der Linden, B.; Makkee, M.; Moulijn, J. A. *J. Catal.* **2001**, *201*, 128.
(45) Zwijnenburg, A.; Goossens, A.; Sloof, W. G.; Crajé, M. W. J.; van der Kraan, A. M.; de Jongh, L. J.; Makkee, M.; Moulijn, J. A. *J. Phys. Chem. B* **2002**, *106*, 9853.
(46) Zwijnenburg, A.; Makkee, M.; Moulijn, J. A. *Appl. Catal., A* **2004**, *270*, 49.
(47) Chou, J.; McFarland, E. W. *Chem. Commun.* **2004**, 1648.
(48) Nijhuis, T. A.; Visser, T.; Weckhuysen, B. M. *Angew. Chem., Int. Ed.* **2005**, *44*, 1115.
(49) Wells, D. H.; Delgass, W. N.; Thomson, K. T. *J. Catal.* **2004**, *225*, 69.
(50) Joshi, A. M.; Delgass, W. N.; Thomson, K. T. *J. Phys. Chem. B* **2005**, *109*, 22392.
(51) Sivadinarayana, C.; Choudhary, T. V.; Daemen, L. L.; Eckert, J.; Goodman, D. W. *J. Am. Chem. Soc.* **2003**, *126*, 38.
(52) Landon, P.; Collier, P. J.; Papworth, A. J.; Kiely, C. J.; Hutchings, G. J. *Chem. Commun.* **2002**, 2058.
(53) Wells, D. H.; Delgass, W. N.; Thomson, K. T. *J. Am. Chem. Soc.* **2004**, *126*, 2956.
(54) Karlsen, E.; Schöffel, K. *Catal. Today* **1996**, *32*, 107.
(55) Neurock, M.; Manzer, L. E. *Chem. Commun.* **1996**, 1133.
(56) Vayssilov, G. N.; van Santen, R. A. *J. Catal.* **1998**, *175*, 170.
(57) Tantanak, D.; Vincent, M. A.; Hillier, I. H. *Chem. Commun.* **1998**, 1031.
(58) Tozzola, G.; Mantegazza, M. A.; Ranghino, G.; Petrini, G.; Bordiga, S.; Ricchiardi, G.; Lamberti, C.; Zullian, R.; Zecchina, A. *J. Catal.* **1998**, *179*, 64.
(59) Sinclair, P. E.; Catlow, C. R. A. *J. Phys. Chem. B* **1999**, *103*, 1084.
(60) Yudanov, I. V.; Gisdakis, P.; Valentin, C. D.; Rösch, N. *Eur. J. Inorg. Chem.* **1999**, 2135.
(61) Munakata, H.; Oumi, Y.; Miyamoto, A. *J. Phys. Chem. B* **2001**, *105*, 3493.
(62) Sever, R. R.; Root, T. W. *J. Phys. Chem. B* **2003**, *107*, 4090.
(63) Limtrakul, J.; Inntam, C.; Truong, T. N. *J. Mol. Catal. A* **2004**, *207*, 137.
(64) Frisch, M. J.; Trucks, G. W.; Schlegel, H. B.; Scuseria, G. E.; Robb, M. A.; Cheeseman, J. R.; Zakrzewski, V. G.; Montgomery, J. A., Jr.; Stratmann, R. E.; Burant, J. C.; Dapprich, S.; Millam, J. M.; Daniels, A. D.; Kudin, K. N.; Strain, M. C.; Farkas, O.; Tomasi, J.; Barone, V.; Cossi, M.; Cammi, R.; Mennucci, B.; Pomelli, C.; Adamo, C.; Clifford, S.; Ochterski, J.; Petersson, G. A.; Ayala, P. Y.; Cui, Q.; Morokuma, K.; Malick, D. K.; Rabuck, A. D.; Raghavachari, K.; Foresman, J. B.; Cioslowski, J.; Ortiz, J. V.; Stefanov, B. B.; Liu, G.; Liashenko, A.; Piskorz, P.; Komaromi, I.; Gomperts, R.; Martin, R. L.; Fox, D. J.; Keith, T.; Al-Laham, M. A.; Peng, C. Y.; Nanayakkara, A.; Gonzalez, C.; Challacombe, M.; Gill, P. M. W.; Johnson, B. G.; Chen, W.; Wong, M. W.; Andres, J. L.; Head-Gordon, M.; Replogle, E. S.; Pople, J. A. *Gaussian 98*, revision A.8; Gaussian, Inc.: Pittsburgh, PA, 1998.
(65) Becke, A. D. *Phys. Rev. A* **1988**, *38*, 3098.
(66) Perdew, J. P.; Chevary, J. A.; Vosko, S. H.; Jackson, K. A.; Pederson, M. R.; Singh, D. J.; Fiolhais, C. *Phys. Rev. B* **1992**, *46*, 6671.
(67) Perdew, J. P.; Chevary, J. A.; Vosko, S. H.; Jackson, K. A.; Pederson, M. R.; Singh, D. J.; Fiolhais, C. *Phys. Rev. B* **1993**, *48*, 4978.
(68) Perdew, J. P.; Burke, K.; Wang, Y. *Phys. Rev. B* **1996**, *54*, 16533.
(69) Hay, P. J.; Wadt, W. R. *J. Chem. Phys.* **1985**, *82*, 270.
(70) Hay, P. J.; Wadt, W. R. *J. Chem. Phys.* **1985**, *82*, 299.

(71) Dunning, J. T. H.; Hay, P. J. In *Modern Theoretical Chemistry*; Schaefer, I. H. F., Ed., Plenum: New York, 1976; Vol. 3.
(72) McQuarrie, D. A.; Simon, J. D. In *Molecular Thermodynamics*; McGuire, A., Ed.; University Science Books: Sausalito, CA, 1999; Chapters 3−7.
(73) Lamberti, C.; Bordiga, S.; Zecchina, A.; Artioli, G.; Marra, G.; Spanò, G. *J. Am. Chem. Soc.* **2001**, *123*, 2204.
(74) van Koningsveld, H.; van Bekkum, H.; Jansen, J. C. *Acta Crystallogr., Sect. B* **1987**, *43*, 127.
(75) Henry, P. F.; Weller, M. T.; Wilson, C. C. *J. Phys. Chem. B* **2001**, *105*, 7452.
(76) Lin, W.; Frei, H. *J. Am. Chem. Soc.* **2002**, *124*, 9292.
(77) Drago, R. S.; Dias, S. C.; McGilvray, J. M.; Mateus, A. L. M. L. *J. Phys. Chem. B* **1998**, *102*, 1508.